

**REMOTE OPERATION OF A  
FARNSWORTH-HIRSCH FUSOR  
FOR PRODUCING D-T  
NEUTRONS**

By

Kyle Craft

A thesis submitted in partial fulfillment of the  
requirements for the degree of

Bachelor of Science

Houghton College

July 2016

Signature of Author.....

Department of Physics  
July 27, 2016

.....

Dr. Mark Yuly  
Professor of Physics  
Research Supervisor

.....

Dr. Kurt Aikens  
Assistant Professor of Physics

**REMOTE OPERATION OF A  
FARNSWORTH-HIRSCH  
FUSOR FOR PRODUCING D-T  
NEUTRONS**

By

Kyle Craft

Submitted to the Department of Physics  
on May 10, 2016 in partial fulfillment of the  
requirement for the degree of  
Bachelor of Science

**Abstract**

The Farnsworth-Hirsch fusor at Houghton College is being modified to allow remote operation. The Farnsworth-Hirsch fusor is a type of inertial electrostatic confinement fusion device that can produce neutrons from deuterium-deuterium fusion reactions and x-rays from high energy electrons. The original Sorensen high voltage power supply has been replaced with a Bertan 815-30N that is able to be controlled remotely through the use of an external analog set voltage. To control and monitor the pressure inside of the chamber, an Apex AX-MC-50SCCM-D mass flow controller and a CCM501 cold-cathode ion gauge are used. LabVIEW code running on a remote computer controls the devices over an Ethernet-to-serial interface. Details of the implementation will be discussed, as well as preliminary results from the remote operation of the fusor.

Thesis Supervisor: Dr. Mark Yuly  
Title: Professor of Physics

## TABLE OF CONTENTS

<b>Chapter 1 Introduction.....</b>	<b>5</b>
<b>1.1 Nuclear Fusion.....</b>	<b>5</b>
<b>1.2 History of Controlled Fusion Research .....</b>	<b>7</b>
1.2.1 Magnetic Confinement .....	7
1.2.2 Inertial Confinement .....	8
1.2.3 Inertial Electrostatic Confinement .....	8
1.2.4 Initial Farnsworth Fusor Designs .....	9
1.2.5 Farnsworth-Hirsch Fusor.....	10
1.2.6 Current Research.....	13
<b>1.3 Motivation of Experiment .....</b>	<b>14</b>
<b>Chapter 2 Theory .....</b>	<b>16</b>
<b>2.1 Overview of Theory.....</b>	<b>16</b>
<b>2.2 Potential Wells.....</b>	<b>16</b>
<b>2.3 Governing Equations for Plasmas.....</b>	<b>18</b>
<b>Chapter 3 Experimental Procedure and Apparatus.....</b>	<b>24</b>
<b>3.1 Fusor Chamber .....</b>	<b>24</b>
<b>3.2 High Voltage System .....</b>	<b>28</b>
3.2.1 External Operation.....	28
3.2.2 Remote Operation of Local Power Supplies and Multimeters .....	31
<b>3.3 Controlling and Monitoring Chamber Pressure.....</b>	<b>36</b>
3.3.1 Remote Operation of Mass Flow Controller.....	36
3.3.2 Calibration of the Mass Flow Controller.....	39
3.3.3 Remote Operation of the Cold-Cathode Ion Gauge .....	39
<b>Chapter 4 Results and Conclusions .....</b>	<b>43</b>
<b>4.1 Results from Low-Pressure Air.....</b>	<b>43</b>
<b>4.2 Conclusions and Future Work.....</b>	<b>46</b>

## TABLE OF FIGURES

Figure 1. Binding energy per nucleon as a function of the atomic mass number .....	6
Figure 2. Original design of the Farnsworth Fusor.....	10
Figure 3. Farnsworth’s second fusor design .....	11
Figure 4. Final design of the Farnsworth-Hirsch fusor from the Hirsch-Meeks patent.....	12
Figure 5. Full fusor design proposed in the Hirsch-Meeks patent. ....	13
Figure 6. The chamber interior. ....	17
Figure 7. Typical potential in a Farnsworth-Fusor. ....	17
Figure 8. Houghton College Farnsworth-Hirsch fusor. ....	25
Figure 9. Fusor-vaccum system.....	26
Figure 10. Electronics for remote operation of the Farnsworth-Hirsch fusor. ....	27
Figure 11. Test circuit for the Bertan power supply. ....	29
Figure 12. Measured current in the test circuit as a function of the set voltage .....	30
Figure 13. Measured voltage in the test circuit.....	31
Figure 14. LabVIEW VI for writing to the PSP 603. ....	32
Figure 15. LabVIEW VI for reading data from the M9803R. ....	33
Figure 16. Second portion of the LabVIEW VI to read from the M9803R. ....	34
Figure 17. A LabVIEW VI that reads two M9803R devices and writes to two PSP 603 devices .....	35
Figure 18. Front panel for the combined LabVIEW VI.....	36
Figure 19. A LabVIEW program that adjusts the mass flow controller .....	38
Figure 20. Pressure as a function of the set-point of the mass flow controller .....	40
Figure 21. LabVIEW VI that turns the high voltage for the pressure gauge and reads pressure .....	41
Figure 22. Front panel for operating the both the mass flow controller and pressure gauge .....	42
Figure 23. Current versus voltage for air at a pressure of 4.8 mTorr.....	44
Figure 24. Output voltage versus set voltage for air at 4.8 mTorr. ....	44
Figure 25. Output voltage versus the pressure for air at 22 kV.....	45
Figure 26. ${}^2\text{H}(d,n){}^3\text{He}$ fusion reaction cross section .....	47

## Chapter 1

### INTRODUCTION

#### 1.1 Nuclear Fusion

Einstein's famous equation  $E = mc^2$  indicates that mass is equivalent to energy. Since this is true, there should be a way to convert some of the mass of an object into energy. While other types of reactions, such as mechanical and chemical reactions, release small amounts of energy, nuclear reactions like fusion and fission deal with the most tightly bound part an atom, the nucleus. Thus, the energy output from a fusion or fission reaction typically far exceeds that of a chemical or mechanical reaction. This thesis focuses on the Farnsworth-Hirsch fusor, a device for releasing energy from nuclear fusion reactions.

The total mass of a nucleus is less than its constituent parts. This difference in mass is accounted for by the binding energy of the nucleus, which holds the nucleus together. The binding energy of a nucleus is given by

$$B = (Zm_p + Nm_n - M)c^2 \quad (1.1)$$

where  $Z$  is the number of protons,  $m_p$  is the mass of the proton,  $N$  is the number of neutrons,  $m_n$  is the mass of the neutron, and  $M$  is the total mass of the nucleus. The binding energy per nucleon,  $B/A$ , where  $A$  is the number nucleons, is the average energy required to remove a nucleon from the nucleus, and depends on the atomic number as shown in Figure 1. Notice that the binding energy per nucleon increases with increasing atomic number up until  ${}^{56}_{26}\text{Fe}$  and then starts to decrease with increasing atomic number. Nuclear fusion takes advantage of this rapid increase seen at low atomic

numbers. By fusing two nuclei with a low binding energy into another nucleus with a higher binding energy, the difference in energy is typically released in the form of kinetic energy of the products, which eventually is degraded simply to heat. This heat can then be converted to electrical energy.

In order to achieve the fusion of the two nuclei, the nuclei must be brought close enough that the strong nuclear force pulls them together, fusing the two nuclei. However, when the two nuclei are brought near each other, the Coulomb force causes a strong repulsion between the two that will slow down and deflect them from each other. Therefore, the kinetic energy of the nuclei needs to be large enough that they can approach within range of the strong force, about 1 fm. At high energies, in order to have a high probability of interacting the nuclei must somehow be confined so that there are many close approaches per unit time.

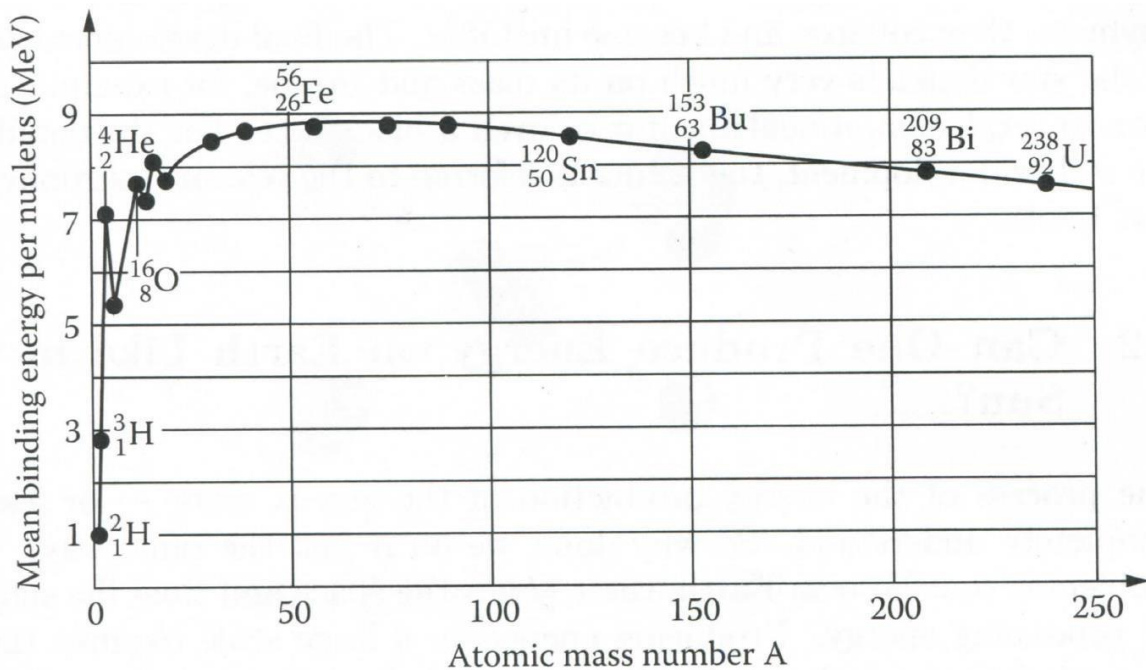


Figure 1. The binding energy per nucleon as a function of the atomic mass number. There is a net energy gain for fusion at lower atomic mass numbers and for fission at high atomic mass numbers. Figure from Ref. [1].

## 1.2 History of Controlled Fusion Research

As stated above, the movement of the nuclei needs to be confined to increase the number of opportunities for interaction, or the probability of interaction. This probability is proportional to a quantity called the cross section of the nuclear reaction. In addition, the kinetic energy of the nuclei must be increased for fusion to occur. At high temperatures, the electrons have enough energy to escape from their atoms and so ionization occurs. A plasma, which is an ionized gas where the positive ions and electrons are not bound together, is formed. These three factors, temperature, the amount of confinement, and the cross section, are the important factors which decide if ignition will occur, where ignition is the point where the fusion reaction is self-sustaining, i.e. the energy released is enough to keep the temperature high enough to keep fusion reactions going.

The three fusion confinement methods that have been studied the most are magnetic confinement fusion, inertial confinement fusion, and inertial electrostatic confinement. All three seek to satisfy Lawson's criterion [2], which defines minimum requirements on the temperature, ion density and confinement time that must be met before the energy released from fusion is greater than the energy put in to maintain the plasma's temperature, resulting in a net release of energy. A brief overview will be given for all three fusion methods, before focusing on inertial electrostatic confinement.

### 1.2.1 *Magnetic Confinement*

Magnetic confinement fusion, as the name implies, confines a plasma using magnetic fields, which is possible because a plasma is charged. One possible way to do this is to use a solenoid with the magnetic field pointing along the axis of the solenoid. This will prevent charged particles in the plasma from colliding with the sides of the solenoid, but the magnetic field does not prevent the particles from exiting the ends of the solenoid. There are two proposed solutions to this problems. One solution is to use magnetic mirrors on the ends of the solenoid. Magnetic mirrors are special magnets that "pinch" the magnetic field lines together on the end of the solenoid, which will often repel approaching ions, reversing their direction. In this way, the plasma can be contained both radially and longitudinally in the solenoid. The problem with this solution is that the confinement is incomplete, some ions can still

escape. Another solution is to wrap the solenoid around into a toroid, connecting the ends. However, in this configuration the ions are not fully contained radially and can drift out to the walls of the solenoid. A possible solution to this is the tokamak, which contains the plasma in a toroidal shape by also creating a poloidal field in such a way so that the ions are always contained and do not collide with the walls of the device. Typical ion densities for this type of confinement are on the order of  $10^{14}$  particles per cubic centimeter while confinement times are usually around 10 seconds [1]. One problem that arises in the tokamak is due to collisions of ions in the plasma. These collisions can push ions to the edges of the tokamak where they collide with the wall.

### 1.2.2 *Inertial Confinement*

Inertial confinement fusion attempts to confine a fuel to very high densities, on the order of  $10^{26}$  ions per cubic centimeter [1]. This is usually done by isotropically bombarding a very small fuel pellet, filled with deuterium and tritium, with high power lasers or ion beams. The shell containing the deuterium-tritium mixture is heated up by the laser and is ablated. The ablation of the shell pushes the deuterium-tritium mixture toward the center of the pellet, greatly increasing the ion density, and confining it for approximately  $10^{-11}$  seconds [1]. With a high ion-density, high temperature, and a short confinement time, fusion can occur in the deuterium-tritium mixture. A problem with this method is anisotropy in implosions and the resulting Rayleigh-Taylor instability [1].

### 1.2.3 *Inertial Electrostatic Confinement*

The last of the three confinement techniques is also inertial in nature, but confines the plasma electrostatically in a potential well. This was originally not thought to be possible according to Earnshaw's theorem [3] which shows that a plasma cannot be contained with an electrostatic field alone because a collection of point charges will only at most have a stable equilibrium in one plane of a three-dimensional coordinate system. The system will fall out of equilibrium through motion in one of the other two planes because it is an unstable equilibrium. However, Earnshaw's theorem assumes that the

point charges are static, which is not the case in inertial electrostatic confinement (IEC). The ions are consistently circulating in the potential well until they collide.

The potential well is typically created using a spherical cathode grid located in a low pressure gas-filled chamber. Positive ions are attracted to the cathode grid and fall into the potential well where, typically, they get trapped because they do not have enough energy to escape the well. The ions then circulate in the potential well until they either collide with another ion or the cathode grid. Since all the ions in the chamber are attracted to the potential well in the center of the chamber, there is a greater chance for collision because of the ion density, which in principle can be as high as  $10^{16}$  ions per cubic centimeter [4]. Before discussing further details about electrostatic confinement, the history of several electrostatic inertial confinement devices will be presented.

#### 1.2.4 *Initial Farnsworth Fusor Designs*

Philo T. Farnsworth patented his first idea for an electrostatic confinement fusor in 1966 [5]. There are a few variations of the design included in this patent. One such design is shown in Figure 2(a). An ion gun attached to the chamber ionizes low pressure gas that fills the chamber. The shell of the chamber is grounded to act as a cathode while a spherical mesh, located in the center, is given a high positive voltage to act as an anode. Because of the anode, electrons are accelerated toward the center. As the electrons approach the center, the Coulomb force slows down the electrons and deflects them away from one another, creating a virtual cathode in the center of the anode grid. The positive ions are then attracted toward the virtual cathode at the center and fall through the anode. Once through the anode, they circulate within it until a collision occurs. A plot of the potential inside of the chamber is shown in Figure 2(b). Notice that there is a potential well in the vicinity of the virtual cathode that is hard to escape.

Two years later, in 1968, Farnsworth filed another patent for new design of the fusor, shown in Figure 3(a) [6]. While the overall concept remained the same, the major change was that the anode and cathode were switched so that the cathode lied inside of the anode. This decision was made because the cathode is relatively impermeable to electrons while still being permeable to positive ions. When positive ions are

introduced into the chamber, similar to the electrons in the first design, they are accelerated to the center of the chamber by the cathode. They are then slowed and deflected from one another near the center forming a virtual anode. The positive ions then oscillate between the two anodes, being accelerated by the cathode. If the potential of the anode is high enough, electrons in the chamber are then accelerated to the center creating a virtual cathode inside of the virtual anode resulting in multiple potential wells. The potential wells created by the virtual cathodes and anodes are shown in Figure 3(b).

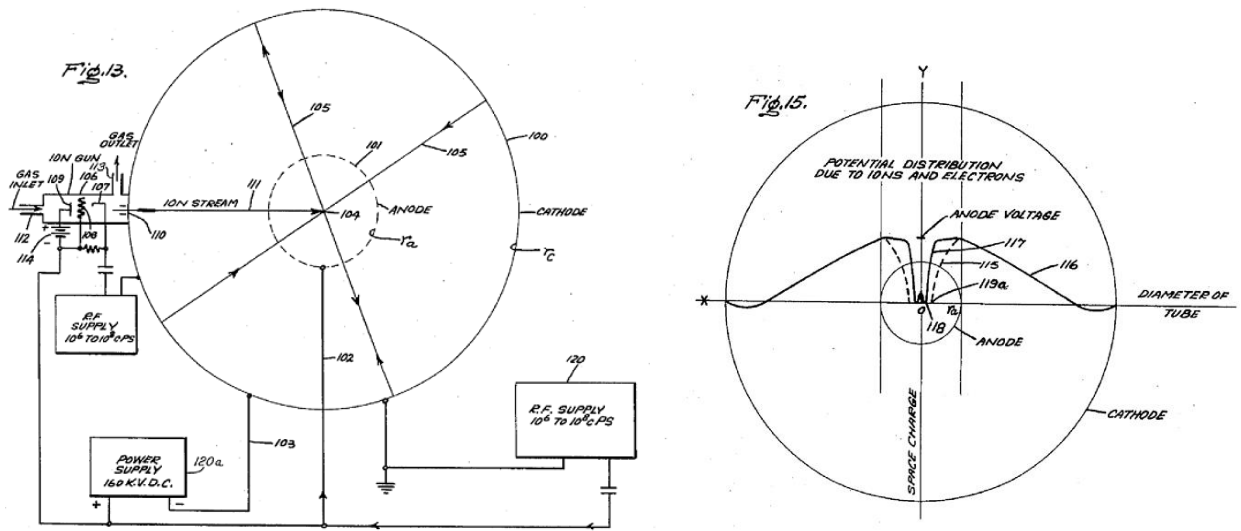


Figure 2. (a) On the left, original design of the Farnsworth Fusor. Positive ions are attracted to the center of the chamber via a virtual cathode that is formed by electrons traveling through the anode. Figure from Ref. [5]. (b) On the right, potential as a function of radius in the original Farnsworth fusor. Electrons attracted to the center are repelled from each other creating a virtual cathode, which results in the potential well (solid black line). Figure from Ref. [5].

### 1.2.5 Farnsworth-Hirsch Fusor

The final change to the design of the Farnsworth fusor came with the patent by Robert Hirsch, who worked with Farnsworth and Gene Meeks in 1970 [7]. There were multiple major changes to the

previous designs of Farnsworth. While the cathode was still located inside of the anode, an additional wire mesh was placed in between them to act as an ion source as shown in Figure 4(a), and a thermionic cathode was added. The thermionic cathode produced electrons that were drawn to the positive high voltage of the ion source grid and then oscillated around it.

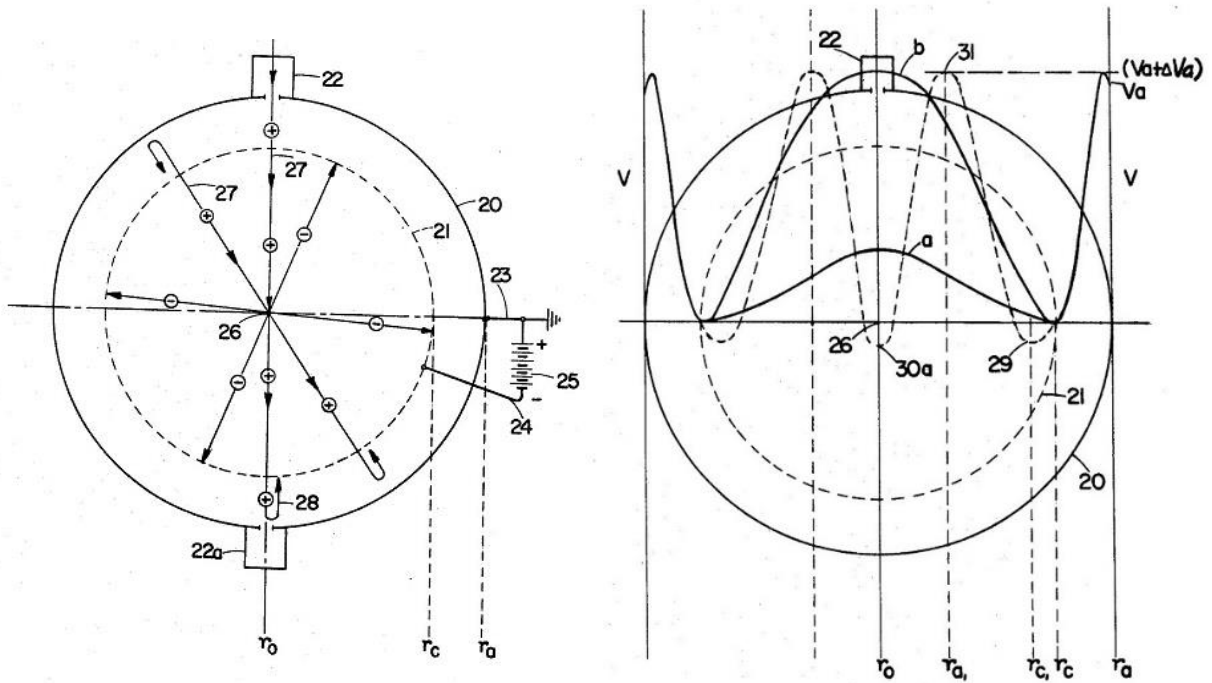


Figure 3. (a) On the left, Farnsworth's second fusor design, where  $r_c$  and  $r_a$  denote the radii of the cathode grid and anode grid respectively. Typical travel paths of the positive ions and electrons are indicated with arrows. Figure from Ref. [6]. (b) On the right, potential as a function of radius for Farnsworth's second design. The two solid lines are potentials due to virtual anodes with line  $b$  being produced from higher current. The dotted line is the potential due to a virtual cathode. The creation of the virtual cathode forms two potential wells, one at  $r_0$  and one at  $r_c$ . Figure from Ref. [6].

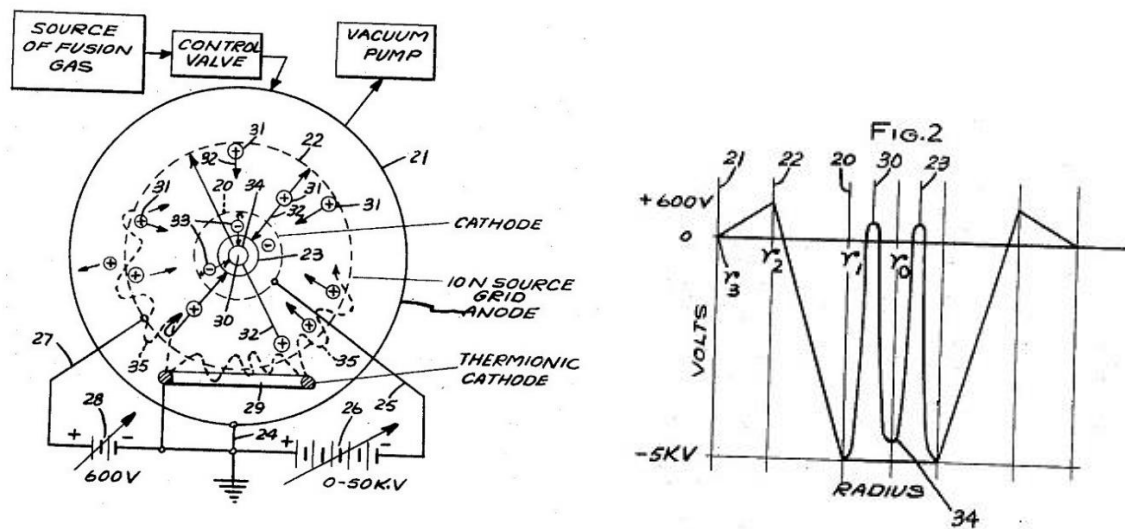


Figure 4. (a) On the left, final design of the Farnsworth-Hirsch fusor from the Hirsch-Meeks patent [7]. Ions were created near the ion source grid by the collision of electrons, produced from the thermionic cathode, with the neutral gas in the chamber. These ions were then attracted to the center of the chamber because of the cathode. Figure from Ref. [7]. (b) On the right, potential distribution inside of the Hirsch-Meeks fusor. By the formation of multiple virtual anodes and cathodes in the center of the fusor, multiple potential wells are formed, in this case two, one at  $r_0$  and one at  $r_1$ . Figure from Ref. [7].

This ion grid source replaced the function of the ion guns in the original designs of Farnsworth. By using this spherical grid to produce ions, the initial ion distribution was more symmetrical around the cathode. In addition, both the cathode and the ion source grid were made more open so that ions could freely flow through them. This reduced the number of electrons and ions lost to collisions with the spherical meshes.

While the design of the fusor changed, as shown in Figure 5, the overall operation remained the same. The positive ions produced from the ion grid source were still accelerated to the center by the cathode where the deceleration and deflection of the ions formed a virtual anode. The ions then oscillated

between the virtual anode at the center and the ion grid source until they either collided with each other or one of the meshes. The potential wells formed by these virtual cathodes and anodes are shown in Figure 4(b), with two potential wells being created from the multiple virtual cathodes and anodes.

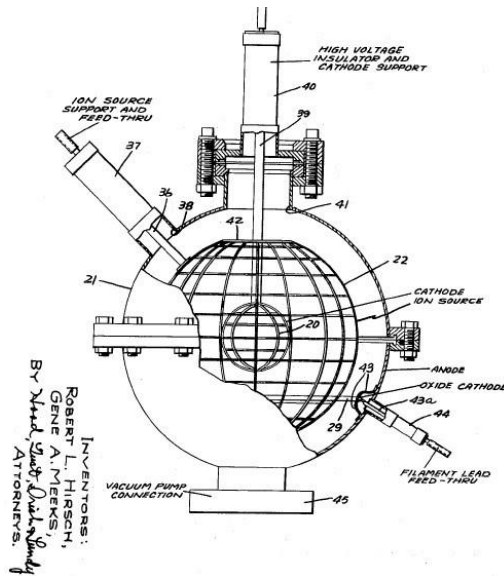


Figure 5. Full fusor design proposed in the Hirsch-Meeks patent. The cathode was a spherical mesh located inside the ion source. Both grids could be moved using the feedthroughs 37 and 40. These feedthroughs also transmitted the high voltage applied to each grid. Figure from Ref. [7].

### 1.2.6 Current Research

Further variations to the fusor have also been proposed and tested, such as the Polywell developed and tested by Robert Bussard at the Energy/Matter Conversion Corporation in the 1990s [8]. The Polywell uses magnets situated around the fusor to confine electrons to the center and form an electrostatic trap for ions. Major current research is occurring both at the University of Wisconsin-Madison [9] as well as the University of Illinois [10]. The University of Wisconsin-Madison has two IEC devices, one with a cylindrical aluminum chamber and another that is a spherical, water-cooled stainless-steel chamber, both

powered by a supply capable of 200 kV. They have been able to achieve a D-D neutron production at a rate of  $1.8 \times 10^8 \text{ s}^{-1}$ . The University of Illinois is currently focusing on IEC using dipole fields to help contain the plasma in the center of the chamber [10].

The Farnsworth-Hirsch fusor's main commercial use is as a neutron source. One example is the neutron generator produced by NSD-Fusion, which was first developed in 1996. Because the generator utilizes IEC, it has several advantages over other neutron sources, such as the absence of a solid target which prevents sputtering, no filament to burn out, a stable neutron output, and the ability to quickly switch the device into high output [11].

The fusor has also seen popularity with amateur experimenters, with Fusor.net [12] providing resources for amateurs to build small scale Farnsworth-Hirsch fusors on their own.

### **1.3 Motivation of Experiment**

At Houghton College, a Farnsworth-Hirsch electrostatic inertial confinement device has been built and is currently being modified to be capable of remote control. The fusor is a stainless steel 0.35 m diameter vacuum chamber, able to be evacuated to about  $10^{-7}$  Torr, with 18 ports of varying sizes. Inside of the chamber are two concentric spherical wire grids composed of stainless steel wire with a smaller 7.0 cm grid is contained inside of the larger 20.3 cm grid. The smaller grid is attached to negative high voltage up to 30,000 V through an electrical feedthrough.

When the fusor is operating, x-rays are produced, and when fusion experiments begin neutrons will also be produced by the nuclear reactions taking place. Neutrons are very difficult to shield and present a radioactive hazard requiring safety precautions including the remote operation of the fusor. Remote operation also allows the possibility of automating the operation of the fusor and data collection in the future.

The Farnsworth-Hirsch fusor will allow for D-D fusion reactions to be studied. One of the big questions surrounding the Farnsworth-Hirsch fusor is whether or not it can realistically meet Lawson's

criterion and generate a net release of energy or at least break even. One theoretical study by T.H Rider [13] making certain realistic assumptions found that inertial electrostatic confinement cannot break even, but experimental verification is still needed.

In any case, the Farnsworth-Hirsch fusor may also be used as a neutron source. At Houghton College, physics students are required to take on an experimental project under the guidance of a professor, and work on this project for several years until they graduate. The IEC device will allow a number of future research projects to be undertaken, including experiments with x-ray fluorescence, where x-rays characteristic of a transition between particular energy level in a particular element are released after a material is excited with high energy x-rays, as well as experiments examining the biological effects of x-rays. Experiments with neutrons such as the measurement of cross-sections using inelastic scattering can also be done with the neutrons produced by the fusor. Finally, multiple experiments examining different properties of plasmas can be done in order to further figure out how IEC works exactly since it is complex.

## Chapter 2

### THEORY

#### 2.1 Overview of Theory

Despite the simplicity of the Farnsworth-Hirsch fusor design, multiple theoretical concepts are required to fully understand the operation of the fusor. In order to create a plasma, ions must be trapped inside the cathode grid. Therefore, an understanding of the potential well is needed in order to describe how the ions are contained. The size and shape of the potential well varies with the ion current in the region. Once a plasma is created, it must be maintained. Therefore, how the plasma reacts to and moves in the electric field must be known in order to maintain a stable plasma. Thus the generation of the potential well and the movement of the plasma will be covered in this chapter.

#### 2.2 Potential Wells

As previously mentioned, in inertial electrostatic confinement a potential well is used to trap ions in a small volume. Presented here is a brief discussion of the dynamics of the potential wells in the Farnsworth-Hirsch fusor.

In the simplified Farnsworth-Hirsch fusor in Figure 6, the cathode grid is held at a high negative voltage, creating a potential well inside the cathode, with the lowest potential being at the center. Positive ions are attracted to this low potential and, unless the ions started with a significant amount of energy, they will not have enough energy to exit out of the well, and will be trapped inside the cathode grid. As the ion current through the center of the fusor is increased by more ions being trapped, the collection of positive charges increases the potential in the center, creating a virtual anode. Ions are attracted to regions of lower potential and thus move away from virtual anode into the potential well between the virtual anode and the cathode grid. Meanwhile free electrons in the chamber are attracted to the virtual

anode and when a significant number of electrons are in the center they create a virtual cathode inside the virtual anode. There are now multiple potential wells inside of the cathode grid that ions can be trapped in as displayed in Figure 7.

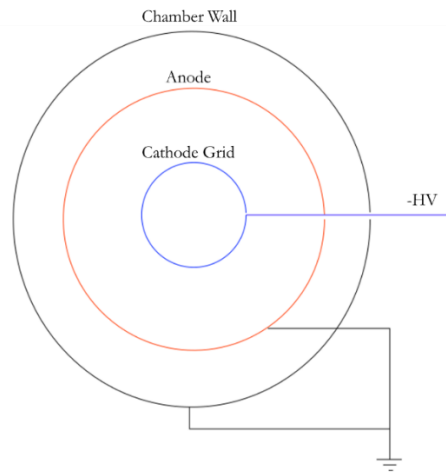


Figure 6. The chamber interior. The blue is the cathode grid placed at a negative high voltage. The red circle is a grounded grid that acts as an anode.

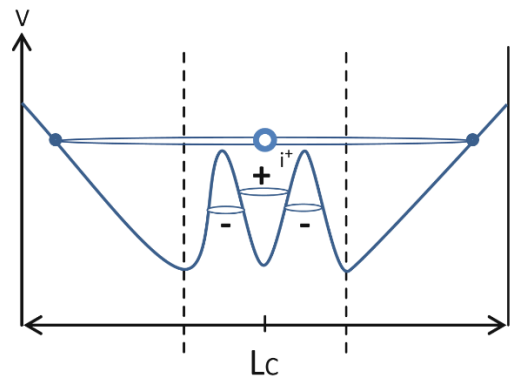


Figure 7. Typical potential in a Farnsworth-Fusor. The  $L_c$  represents the center of the chamber. Notice the two potential wells formed, one at the center and one at the dotted line. Figure from Ref. [4].

### 2.3 Governing Equations for Plasmas

The ions in a plasma follow governing equations primarily influenced by the Lorentz force, since the ions are charged. These equations can be applied to every ion in the plasma, yielding the exact equations for the motion of the plasma. Because the number of ions in a plasma is large, usually only the average motion of the ions is important. Thus, after deriving the exact equations, an average will be taken to yield the measurable macroscopic characteristics of the plasma.

The Klimontovich equation is one of the governing equations for a plasma and is derived here following the derivation of D. R. Nicolson [14]. The Klimontovich equation will then be used to obtain the average equation for the plasma.

Consider a single ion that has a spatial trajectory vector  $\mathbf{X}_1(t)$  that describes its position in three-dimensional space at successive times  $t$ . This ion also has a velocity vector  $\mathbf{V}_1(t)$  that gives its velocity at successive times  $t$ . Let  $N(\mathbf{x}, \mathbf{v}, t)$  be the ion “density” at the location  $(\mathbf{x}, \mathbf{v}, t)$  in the six-dimensional phase space for a single ion which is given by

$$N(\mathbf{x}, \mathbf{v}, t) = \delta[\mathbf{x} - \mathbf{X}_1(t)]\delta[\mathbf{v} - \mathbf{V}_1(t)] \quad (2.1)$$

where  $\delta[\mathbf{x} - \mathbf{X}_1(t)] \equiv \delta(x - X_1)\delta(y - Y_1)\delta(z - Z_1)$  and similarly with  $\delta[\mathbf{v} - \mathbf{V}_1(t)]$ . We call this a density because when it is integrated over volume it yields the total number of ions. Note that  $\mathbf{X}_1(t)$  and  $\mathbf{V}_1(t)$  are with respect to the particle so they are Lagrangian, while  $\mathbf{x}$  and  $\mathbf{v}$  are with respect to a fixed coordinate plane and are thus Eulerian. The general form for the ion density  $N_s$  of ion  $s$  given  $N_0$  total ions of type  $s$  is

$$N_s(\mathbf{x}, \mathbf{v}, t) = \sum_{i=1}^{N_0} \delta[\mathbf{x} - \mathbf{X}_i(t)]\delta[\mathbf{v} - \mathbf{V}_i(t)] \quad (2.2)$$

where  $s$  denotes the kind, or species, of ion and  $i$  is summed over every ion of type  $s$ . Then, if there are multiple species of ions the total density  $N$  is given by

$$N(\mathbf{x}, \mathbf{v}, t) = \sum_s N_s(\mathbf{x}, \mathbf{v}, t). \quad (2.3)$$

The definition of velocity is

$$\dot{\mathbf{X}}_i(t) = \mathbf{V}_i(t). \quad (2.4)$$

Newton's second law applied to the Lorentz force as a function of position and time gives the force on an ion  $i$  of species  $s$ ,

$$\mathbf{F}_i(t) = m_s \dot{\mathbf{V}}_i = q_s \mathbf{E}^m[\mathbf{X}_i(t), t] + \frac{q_s}{c} \mathbf{V}_i(t) \times \mathbf{B}^m[\mathbf{X}_i(t), t] \quad (2.5)$$

where  $q_s$  is the charge of an ion species, and the superscript  $m$  denotes the total field from both the externally applied fields combined with the microscopic fields, the fields “self-consistently produced by the point particles themselves” [10]. We also define the microscopic charge density

$$\rho^m(\mathbf{x}, t) = \sum_s q_s \int d\mathbf{v} N_s(\mathbf{x}, \mathbf{v}, t) \quad (2.6)$$

while the microscopic current is

$$\mathbf{J}^m(\mathbf{x}, t) = \sum_s q_s \int d\mathbf{v} \mathbf{v} N_s(\mathbf{x}, \mathbf{v}, t). \quad (2.7)$$

To get the exact equation of motion, the time derivative of  $N_s$ , given by Equation 2.2 is taken

$$\frac{\partial N_s(\mathbf{x}, \mathbf{v}, t)}{\partial t} = \sum_{i=1}^{N_0} \frac{\partial}{\partial t} \{ \delta[\mathbf{x} - \mathbf{X}_i(t)] \delta[\mathbf{v} - \mathbf{V}_i(t)] \} \quad (2.8)$$

and the result is

$$\begin{aligned} \frac{\partial N_s(\mathbf{x}, \mathbf{v}, t)}{\partial t} = & - \sum_{i=1}^{N_0} \dot{\mathbf{X}}_i \cdot \nabla_{\mathbf{x}} \delta[\mathbf{x} - \mathbf{X}_i(t)] \delta[\mathbf{v} - \mathbf{V}_i(t)] \\ & - \sum_{i=1}^{N_0} \dot{\mathbf{V}}_i \cdot \nabla_{\mathbf{v}} \delta[\mathbf{x} - \mathbf{X}_i(t)] \delta[\mathbf{v} - \mathbf{V}_i(t)] \end{aligned} \quad (2.9)$$

where  $\nabla_{\mathbf{x}} \equiv \left( \frac{\partial}{\partial x}, \frac{\partial}{\partial y}, \frac{\partial}{\partial z} \right)$  and  $\nabla_{\mathbf{v}} \equiv \left( \frac{\partial}{\partial v_x}, \frac{\partial}{\partial v_y}, \frac{\partial}{\partial v_z} \right)$ . Using Equations 2.4 and 2.5 we can rewrite Equation 2.9 in terms of the electric and magnetic fields

$$\begin{aligned} \frac{\partial N_s(\mathbf{x}, \mathbf{v}, t)}{\partial t} = & - \sum_{i=1}^{N_0} \mathbf{V}_i \cdot \nabla_{\mathbf{x}} \{ \delta[\mathbf{x} - \mathbf{X}_i(t)] \delta[\mathbf{v} - \mathbf{V}_i(t)] \} \\ & - \sum_{i=1}^{N_0} \left\{ \frac{q_s}{m_s} \mathbf{E}^m[\mathbf{X}_i(t), t] + \frac{q_s}{m_s c} \mathbf{V}_i(t) \times \mathbf{B}^m[\mathbf{X}_i(t), t] \right\} \\ & \cdot \nabla_{\mathbf{v}} \delta[\mathbf{x} - \mathbf{X}_i(t)] \delta[\mathbf{v} - \mathbf{V}_i(t)]. \end{aligned} \quad (2.10)$$

Using the property of the Dirac delta function

$$a\delta(a - b) = b\delta(a - b) \quad (2.11)$$

we can replace  $\mathbf{V}_i$  and  $\mathbf{X}_i$  with  $\mathbf{v}$  and  $\mathbf{x}$  respectively outside of the delta function. Thus Equation 2.10 becomes

$$\begin{aligned} \frac{\partial N_s(\mathbf{x}, \mathbf{v}, t)}{\partial t} &= -\mathbf{v} \cdot \nabla_{\mathbf{x}} \sum_{i=1}^{N_0} \delta[\mathbf{x} - \mathbf{X}_i(t)] \delta[\mathbf{v} - \mathbf{V}_i(t)] \\ &\quad - \left\{ \frac{q_s}{m_s} \mathbf{E}^m[\mathbf{x}, t] + \frac{q_s}{m_s c} \mathbf{v} \times \mathbf{B}^m[\mathbf{x}, t] \right\} \\ &\quad \cdot \nabla_{\mathbf{v}} \sum_{i=1}^{N_0} \delta[\mathbf{x} - \mathbf{X}_i(t)] \delta[\mathbf{v} - \mathbf{V}_i(t)]. \end{aligned} \quad (2.12)$$

We can replace the summations with the total plasma density  $N_s$ , Equation (2.2), to get

$$\frac{\partial N_s(\mathbf{x}, \mathbf{v}, t)}{\partial t} + \mathbf{v} \cdot \nabla_{\mathbf{x}} N_s + \frac{q_s}{m_s} \left\{ \mathbf{E}^m[\mathbf{x}, t] + \frac{\mathbf{v}}{c} \times \mathbf{B}^m[\mathbf{x}, t] \right\} \cdot \nabla_{\mathbf{v}} N_s = 0 \quad (2.13)$$

which is the exact Klimontovich equation for a single ion species  $s$ . However, it would be more useful to have an averaged equation because we only care about the macroscopic characteristics of the plasma.

We do this by defining

$$f_s(\mathbf{x}, \mathbf{v}, t) \equiv \langle N_s(\mathbf{x}, \mathbf{v}, t) \rangle \quad (2.14)$$

where  $\langle \rangle$  denotes an ensemble average. We do not give a specific average since the average depends on the ensemble chosen to describe the system. Having this, we define small perturbations from the ensemble average  $\delta N_s$ ,  $\delta \mathbf{E}$ , and  $\delta \mathbf{B}$  by

$$N_s(\mathbf{x}, \mathbf{v}, t) = f_s(\mathbf{x}, \mathbf{v}, t) + \delta N_s(\mathbf{x}, \mathbf{v}, t) \quad (2.15)$$

$$\mathbf{E}^m(\mathbf{x}, t) = \mathbf{E}(\mathbf{x}, t) + \delta \mathbf{E}(\mathbf{x}, t) \quad (2.16)$$

and

$$\mathbf{B}^m(\mathbf{x}, t) = \mathbf{B}(\mathbf{x}, t) + \delta\mathbf{B}(\mathbf{x}, t) \quad (2.17)$$

where  $\mathbf{B} \equiv \langle \mathbf{B}^m \rangle$ ,  $\mathbf{E} \equiv \langle \mathbf{E}^m \rangle$  and  $\langle \delta N_s \rangle = \langle \delta \mathbf{E} \rangle = \langle \delta \mathbf{B} \rangle = 0$ . Using the definitions and ensemble averaging yields

$$\frac{\partial f_s(\mathbf{x}, \mathbf{v}, t)}{\partial t} + \mathbf{v} \cdot \nabla_{\mathbf{x}} f_s + \frac{q_s}{m_s} \left\{ \mathbf{E} + \frac{\mathbf{v}}{c} \times \mathbf{B} \right\} \cdot \nabla_{\mathbf{v}} f_s = -\frac{q_s}{m_s} \langle \left( \delta \mathbf{E} + \frac{\mathbf{v}}{c} \times \mathbf{B} \right) \cdot \nabla_{\mathbf{v}} \delta N_s \rangle \quad (2.18)$$

which is the form of the plasma kinetic equation. This equation can be used to describe the average ion density for a given location in a plasma if given the average  $\mathbf{E}$  and  $\mathbf{B}$  fields. This equation can be further simplified to make Equation 2.18 easier to work with. The right side of the equation depends on the individual particles of the plasma, which are the source of the collisional effects, while the left side represents the collective effects in the plasma. Equation 2.18 can be approximated by neglecting collisional effects in the plasma since the collective effects are much greater. In addition, this experiment deals with low-pressure plasmas, so the number of collisions occurring is small. Making these approximations yields

$$\frac{\partial f_s(\mathbf{x}, \mathbf{v}, t)}{\partial t} + \mathbf{v} \cdot \nabla_{\mathbf{x}} f_s + \frac{q_s}{m_s} \left\{ \mathbf{E} + \frac{\mathbf{v}}{c} \times \mathbf{B} \right\} \cdot \nabla_{\mathbf{v}} f_s = 0 \quad (2.19)$$

which is the Vlasov equation. One popular numerical method for solving the Vlasov equation is the Particle in Cell, or PIC, method. In this method, the initial distribution function  $f_s$  is discretized into macro-particles which are then advanced in time according to the Vlasov equation. A numerical solver can be used to solve the coupled Maxwell equations to determine the magnetic and electric fields at the

location of the macro-particles for the next time step. In this way, the position and velocity of the macro-particles can be simulated to get an idea for how the plasma will behave [14].

## Chapter 3

### EXPERIMENTAL PROCEDURE AND APPARATUS

In this chapter, a brief introduction to the Houghton College Farnsworth-Hirsch fusor design is given. The changes made for remote operation will then be discussed in detail. This will include the process of operating the fusor remotely through the use of LabVIEW virtual instruments.

#### 3.1 Fusor Chamber

The design of the Farnsworth-Hirsch fusor, pictured in Figure 8, remains largely unchanged from the design in Figure 9, which is discussed in detail in Ref. [16], so only a brief description will be given here. The fusor consists of a stainless steel 0.35 m diameter vacuum chamber with 18 ports of varying sizes. Some of the ports are used for viewing the inside of the chamber, other ports have sensors or feedthroughs attached, and one has a thin Mylar window which allows x-rays to exit the chamber to be used for other experiments. The vacuum chamber is connected on the bottom to a Varian model 0159 diffusion pump, with a liquid nitrogen cold trap in between. Attached to the diffusion pump is an Altec model ZM2008A rotary forepump used to evacuate the chamber to around  $1 \times 10^{-3}$  Torr, after which the diffusion pump further evacuates the chamber to the order of  $10^{-7}$  Torr.

Inside of the chamber are two concentric spherical wire grids composed of 0.63 mm diameter 304 stainless steel wire. The smaller 7.0 cm diameter grid, composed of three 7.0 cm rings, is contained inside of the larger 20.3 cm diameter grid, composed of two 20.3 cm rings and two 15.2 cm rings, and the position of both grids can be moved using separate linear motion feedthroughs. The smaller grid is connected to an electrical feedthrough on which can be attached to negative high voltage while the other grid is grounded to the chamber wall.

In order to monitor the pressure inside of the chamber, multiple pressure sensors are used. For pressures down to  $1 \times 10^{-3}$  Torr, a Granville-Phillips Convectron pirani gauge is used to measure the pressure. Once the pressure is down in this range, either a Duniway Stockroom Corp. I-100-K hot cathode ion gauge or an InstruTech CCM501 cold-cathode ion gauge can be used to measure lower pressures. During operation of the fusor, the CCM501 is preferred due to its ruggedness, while both the hot-cathode ion gauge and pirani are not used in order to prevent damage to the sensitive electronics.



Figure 8. The Houghton College Farnsworth-Hirsch fusor apparatus. Both the Apex AX-MC-50SCCM-D mass flow controller (bottom right, black) and the InstruTech CCM501 cold-cathode ion gauge (top left, yellow) can be seen here.

In order to operate the fusor remotely, multiple changes had to be made. These changes involved replacing or adding devices to allow the fusor to be controlled remotely. The most notable changes are the replacement of the Sorensen high voltage power supply with a Bertan Series 815 -30N high voltage power supply, adding a mass flow controller in order to regulate the pressure inside of the chamber remotely and the remote operation of a cold-cathode ion gauge.

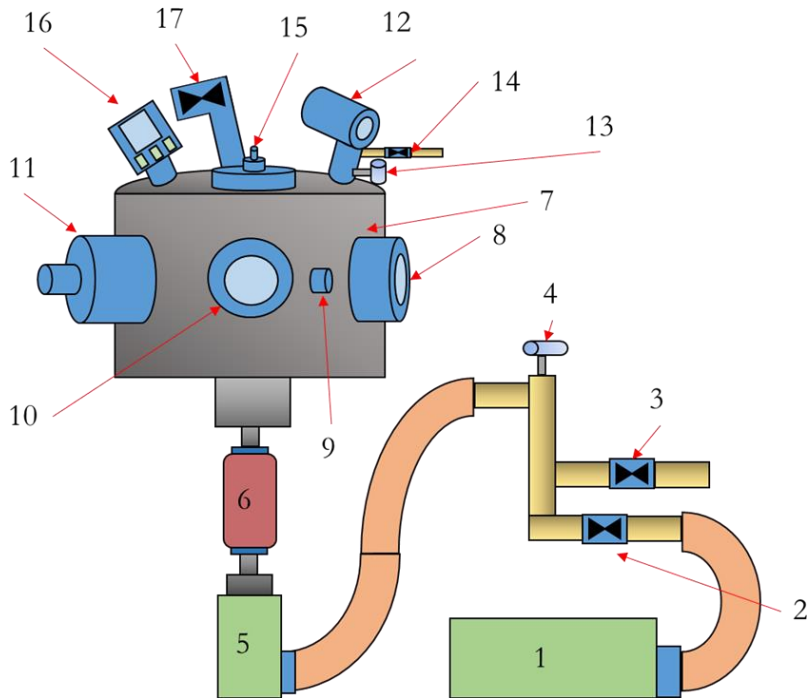


Figure 9. The fusor-vacuum system. The forepump (1) is used to evacuate the chamber to between  $10^{-2}$  and  $10^{-3}$  Torr. Valve (2) allows the forepump to pump from the chamber. The up-to-air valve (3) allows air to enter the vacuum system. A pirani gauge (4) measures the air pressure in the foreline. Pressures down to  $10^{-7}$  Torr are obtained using the diffusion pump (5) and the cold trap (6). The vacuum chamber (7) has various ports such as a viewport (8), a 2.75" conflat port (9), another viewport (10) and a 8" conflat port adapted to 2.75" conflat port (11). A hot cathode ion gauge (12) and a pirani gauge (13) monitor the chamber pressure. The up-to-air valve (14) is attached at this site as well. Port 17 (15) contains the electrical feedthrough and linear motion feedthrough for the outer spherical grid. A CCM501 cold cathode ion gauge (16) is mounted on port 15. A variable leak valve is attached to an angle valve on port 16 (17). Some ports not displayed here are port 2 that has a linear motion feedthrough for the inner grid as well as port 8, which can be used to measure x-rays through a Mylar window. Figure from Ref. [15].

The set-up of the electronics to operate the fusor remotely is shown in Figure 10. The three components that must be controlled are the Bertan Series 815 -30N high voltage power supply, the Apex AX-MC-50SCCM-D mass flow controller, and the InstruTech CCM501 cold-cathode ion gauge. The Bertan

Series 815 -30N high voltage power supply is controlled using two Instek PSP 603 power supplies to change the set point voltage and current limit and two Mastech M9803R multimeters to monitor the output voltage and current. All four devices are connected to the high voltage power supply through one DB-25 cable. The power supplies and multimeters communicate through RS-232 to a Digi Portserver TS4 MEI, which allows the devices to be controlled from a remote computer through the Ethernet network. The Apex AX-MC-50SCCM-D mass flow controller and the InstruTech CCM501 cold cathode ion gauge communicate with a separate Digi Portserver TS4 MEI through RS-232 and RS-485, respectively. These two devices can then be also controlled on a remote computer. On the computer, one LabVIEW virtual instrument is used to control the power supplies and multimeters while another separate LabVIEW virtual instrument is used to control the mass flow controller and cold cathode ion gauge. The settings for all of the serial connections can be seen in Table 1.

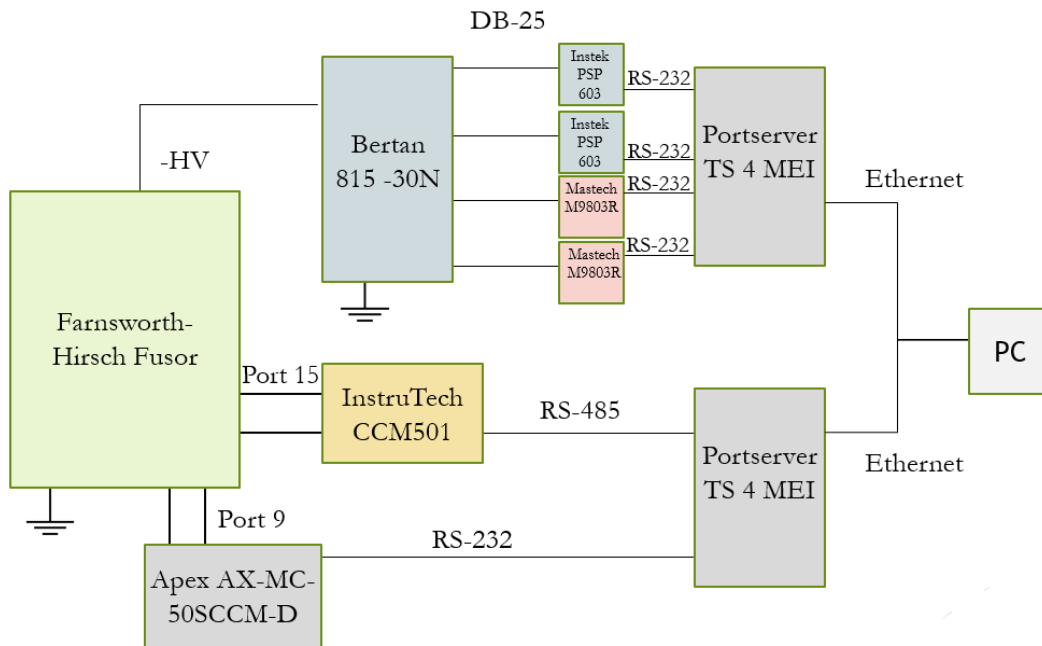


Figure 10. Electronics for remote operation of the Farnsworth-Hirsch fusor. The Bertan 815 -30N high voltage power supply is connected to two supplies and two multimeters using a DB-25 cable, with two wires of the DB-25 going to each supply/multimeter. All devices are connected to a computer where they can be controlled using LabVIEW programs.

Table 1. Settings for the RS-232/RS-485 connections for the Instek PSP 603, Mastech M9803, AX-MC-50SCCM-D, and InstruTech CCM501.

	Instek PSP 603	Mastech M9803	Apex AX-MC-50SCCM-D	InstruTech CCM501
Baud Rate	2400	9600	19,200	19,200
Data Bits	8	7	8	8
Parity	None	None	None	None
Stop Bits	1	2	1	1
Flow Control	None	None	None	None

## 3.2 High Voltage System

High voltage is supplied to an electrical feedthrough by a Bertan Series 815 -30N high voltage power supply. The power supply is capable of producing up to 30,000 V of negative high voltage and a current up to 3.3 mA. This power supply was chosen because it can to be controlled remotely by two 0-5V power supplies via a DB-25 cable.

### 3.2.1 External Operation

The Bertan high voltage power supply is operated remotely by applying voltages to pins 1, 2, 14, and 15 of a DB25 connector on the front panel of the device (see Table 2). This was done using two Instek PSP 603 power supplies that provide 0-5 V across the pins. One power supply provides a voltage across pins 1 and 2, with the positive voltage going to pin 1 and ground going to pin 2. This controls the voltage of the Bertan power supply with 0-5 VDC on the PSP 603 corresponding to 0 to negative 30,000 V on the Bertan. The other power supply does the same for pins 14 and 15, with the positive voltage going to pin 14 and ground going to pin 15. This sets the current limit of the Bertan with 0-5 VDC on the PSP 603 corresponding to 0-3.3 mA on the Bertan. The current and voltage can be monitored using external multimeters across pins 4 and 5 for voltage and pins 17 and 18 for current. This is done using two Mastech M9803R multimeters.

Table 2. The pinout for the Bertan high voltage power supply. A plus sign indicates positive voltage, while a minus sign indicates ground.

Pin	Function
1	$V_{OUT}$ Program Input (+)
2	$V_{OUT}$ Program Input (-)
4	$V_{OUT}$ Program Monitor
5	Common ( $V_{MON}$ Return)
10	Logic Common
11	Enable Input
14	$I_{OUT}$ Program Input (+)
15	$I_{OUT}$ Program Input (-)
17	$I_{OUT}$ Program Monitor
18	Common ( $I_{MON}$ Return)

In order to confirm that the 0-5 VDC correspondence was linear, the Bertan power supply was tested with the circuit in Figure 11. By measuring the current in the circuit, the voltage of the Bertan was determined for each given control voltage supplied by the PSP 603. To originally measure the current, an analog microammeter was used for its durability, but was switched to a digital multimeter for more precision. The measurements from the analog microammeter agreed with the digital multimeter so the multimeter was used. Once the circuit was set up, the PSP 603 controlling the current was set to 5 VDC to ensure that the current did not limit the voltage output by the Bertan. The PSP 603 that controlled the voltage was increased in increments of 0.5 V from 0 V to 3.5 V and then incremented by 0.1 V up to 4.0 V. A final measurement was taken at 4.5 V, but was not increased any higher for safety concerns because the amount of discharge occurring around the resistor chain indicated sparking was imminent.

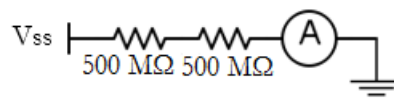


Figure 11. Test circuit for the Bertan power supply. Both resistors were 1.5 W resistors. Since the voltage being applied was between 0 and negative 30,000 V, using this circuit the current measured was between 0 and 3  $\mu\text{A}$ , which gave the voltage being applied using Ohm's Law.

The measured currents are presented in Figure 12, while the calculated voltages are shown in Figure 13. Notice that the relationship between the current and control voltage is nearly linear until around 3.5 V, when the current starts to increase more quickly. This is thought to be due to the current not flowing through the resistors. At higher control voltages (and thus high output voltages from the Bertan), a noticeable electrical corona discharge could be seen. Thus some current bypassed the resistors resulting in a higher measured current than what would be produced if there was not any discharge. This is especially apparent when looking at the measured voltage as a function of the predicted voltage. The predicted voltage was calculated by assuming a linear relationship between the 0-5 VDC from the PSP 603 and the 0-30,000 V output by the Bertan. At a predicted voltage of 24,000 V the “actual voltage” measured is already at 30,000 V, the maximum voltage that the Bertan produces. At a predicted voltage of 27,000 V the measured voltage is approximately 38,000 V, much higher than the maximum output of the Bertan. Of course, the “actual voltage” is much less, because the actual current flowing through the resistors is much less than the measured current.

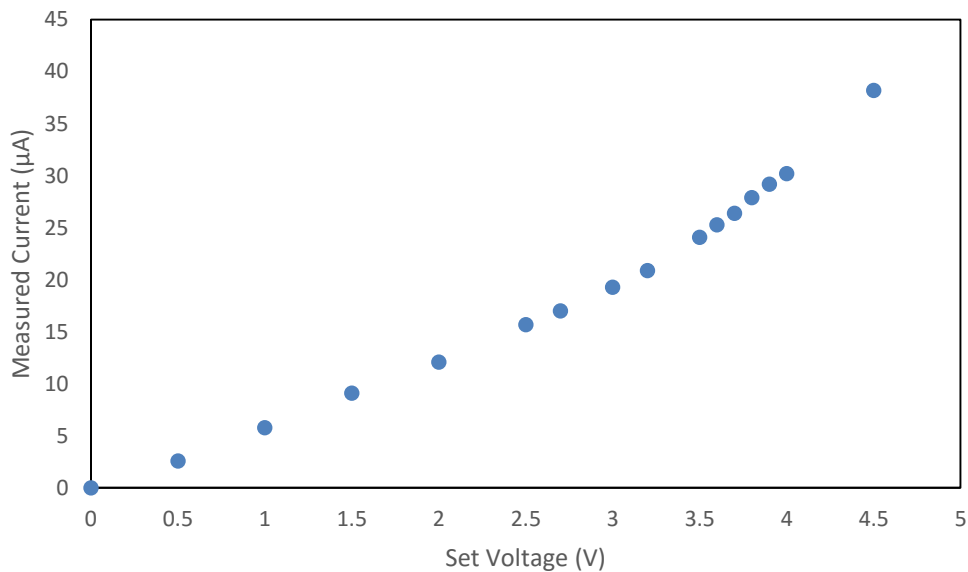


Figure 12. Measured current in the test circuit as a function of the set voltage. A linear relationship between the voltage and current is expected.

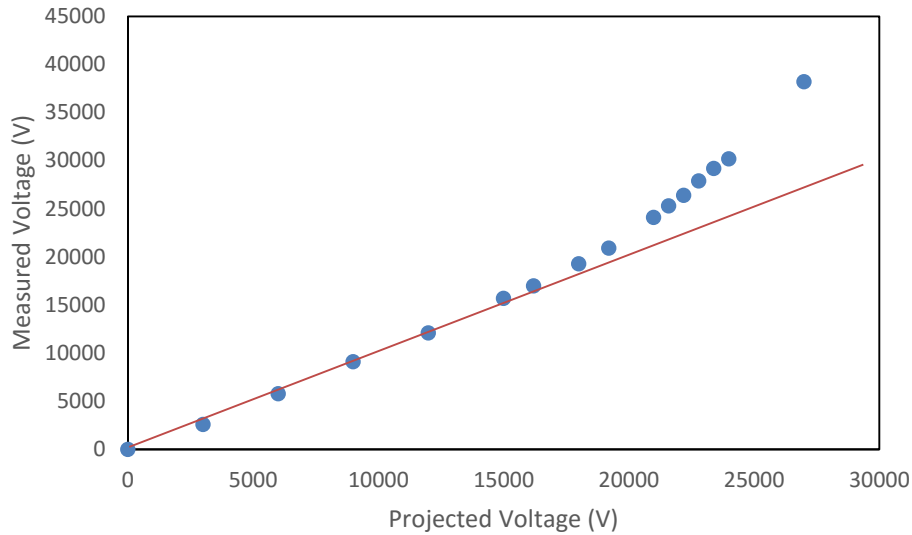


Figure 13. Measured voltage versus the projected voltage of the test circuit, where the projected voltage is the voltage expected from the linear relationship. This expected linear relationship is indicated by the red line. Voltages were calculated using the currents in Figure 12.

### 3.2.2 Remote Operation of Local Power Supplies and Multimeters

Although the Bertan can be controlled and monitored locally with the 0-5 VDC power supplies and multimeters, these devices can also be controlled using a serial interface. The PSP 603 and M9803R are controlled using RS-232 from a Digi Portserver TS 4 MEI that itself communicates with a computer via a local Ethernet network.

To control the PSP 603, a voltage in the form of ASCII digits along with termination characters are written to the device by the LabVIEW virtual instrument shown in Figure 14. The PSP 603 can be controlled through 25 different control codes for reading and changing different parameters of the device. The only code used for this application is \*SV. When it receives the message “SV xx.xx”, where “x” is the ASCII code for the digit 0-9, the PSP-603 sets its voltage to “xx.xx”. Every command sent to the device must end with a carriage return, so “\r” is appended to the end as well.

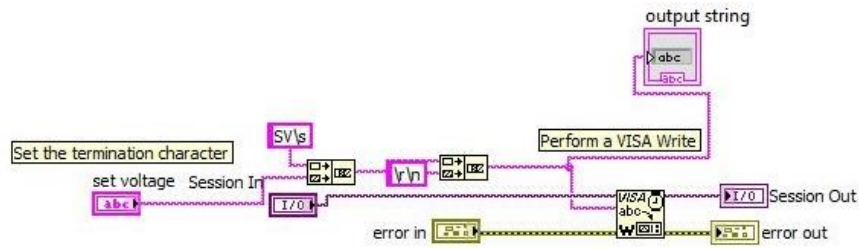


Figure 14. LabVIEW VI for writing to the PSP 603. An ASCII string is input for the voltage desired. The command “SV” used to indicate a change in voltage is prepended while the termination characters are appended. This string is then written to the device.

Reading voltages from the M9803R is slightly more complicated. The first portion of the LabVIEW virtual instrument used is shown in Figure 15 while the second portion is shown in Figure 16. As seen in Figure 15, the serial port is first configured with the correct baud rate, number of data bits, flow control parity, and stop bits. Data are then read in from the device. When reading the M9803R, sometimes a timeout error occurs due to the device continuously outputting data while the LabVIEW VI is not continuously reading. This results in the LabVIEW VI trying to sometimes read in the middle of a string being output by the M9803R. This error condition is checked using if statements. If no error is found, the program exits the while loop. If the error is found, then the device keeps reading until either there is no error, at which point the while loop is exited with the string read. If the error has occurred more than 30 times in a row the program stops. The string received is then parsed, separating out bytes 2, 3, 4, 5, and 8 of the value received, as shown in Figure 16. Bytes 2, 3, 4, and 5 bytes correspond to digits of the voltage displayed on the screen of the multimeter in reverse order, so byte 5 represents the first digit, byte 4 the second, and so on. Finally the last byte of the string corresponds to the magnitude of the voltage displayed, where the order of magnitude is  $10^{(byte-4)}$  with 0 being the lowest order of magnitude and 9 being the highest. As an example, consider if the digits on the screen were 1234. Then if the last byte was 0, the number of the screen would be 0.1234 V, while if the last byte was 9 then  $1234 \times 10^5$  would be on the screen. Both sub VIs are combined in one VI shown in Figure 17, which writes to two PSP 603 devices and reads two M9803R devices, with the front panels

being shown in Figure 18. The voltages from the M9803R devices are calculated in the formula nodes using the bytes parsed.

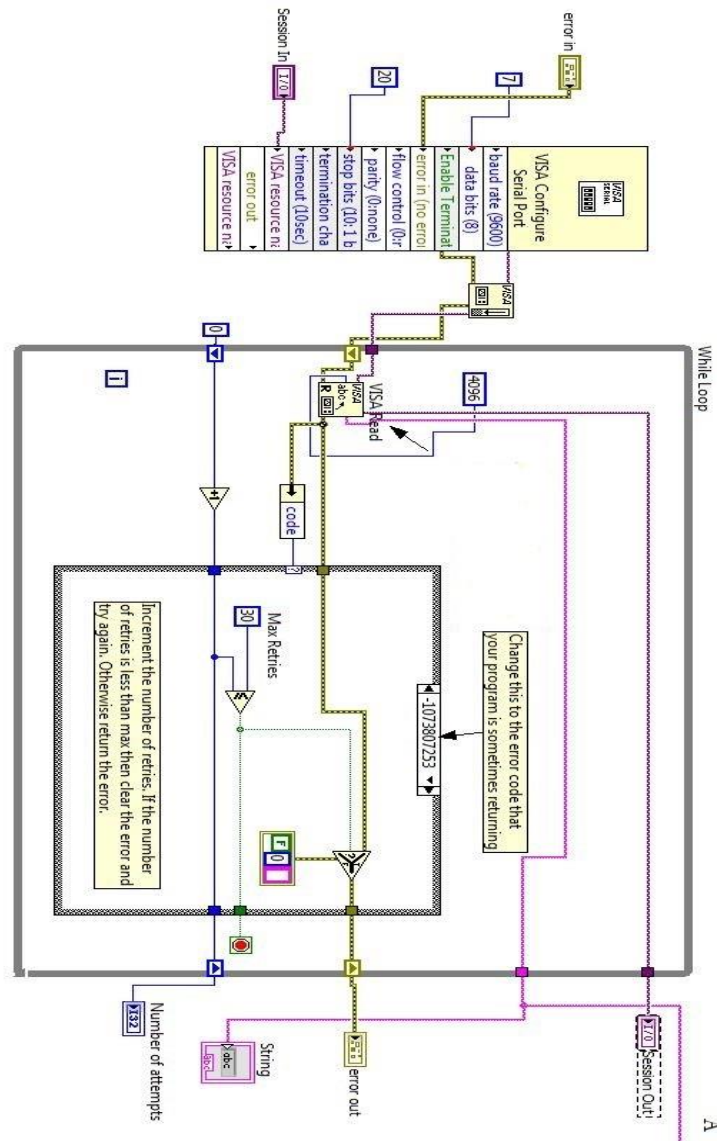


Figure 15. LabVIEW VI for reading data from the M9803R. The serial port is first configured with the correct settings. Afterwards, a string is read from the device. The program checks for a frame error and if one is found, the program will attempt to read a string again up until 30 times after which the program will stop.

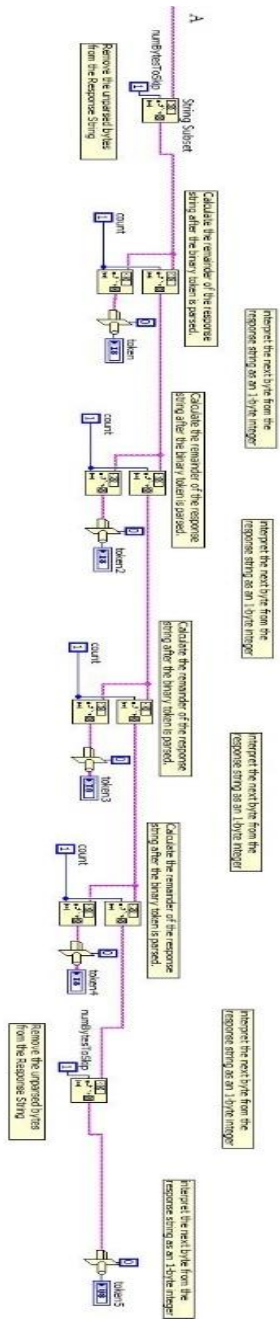


Figure 16. Second portion of the LabVIEW VI to read from the M9803R. The data value read is parsed into individual bytes discarding any bytes not needed. After being parsed, the bytes are converted to an 8 bit integer for later use.

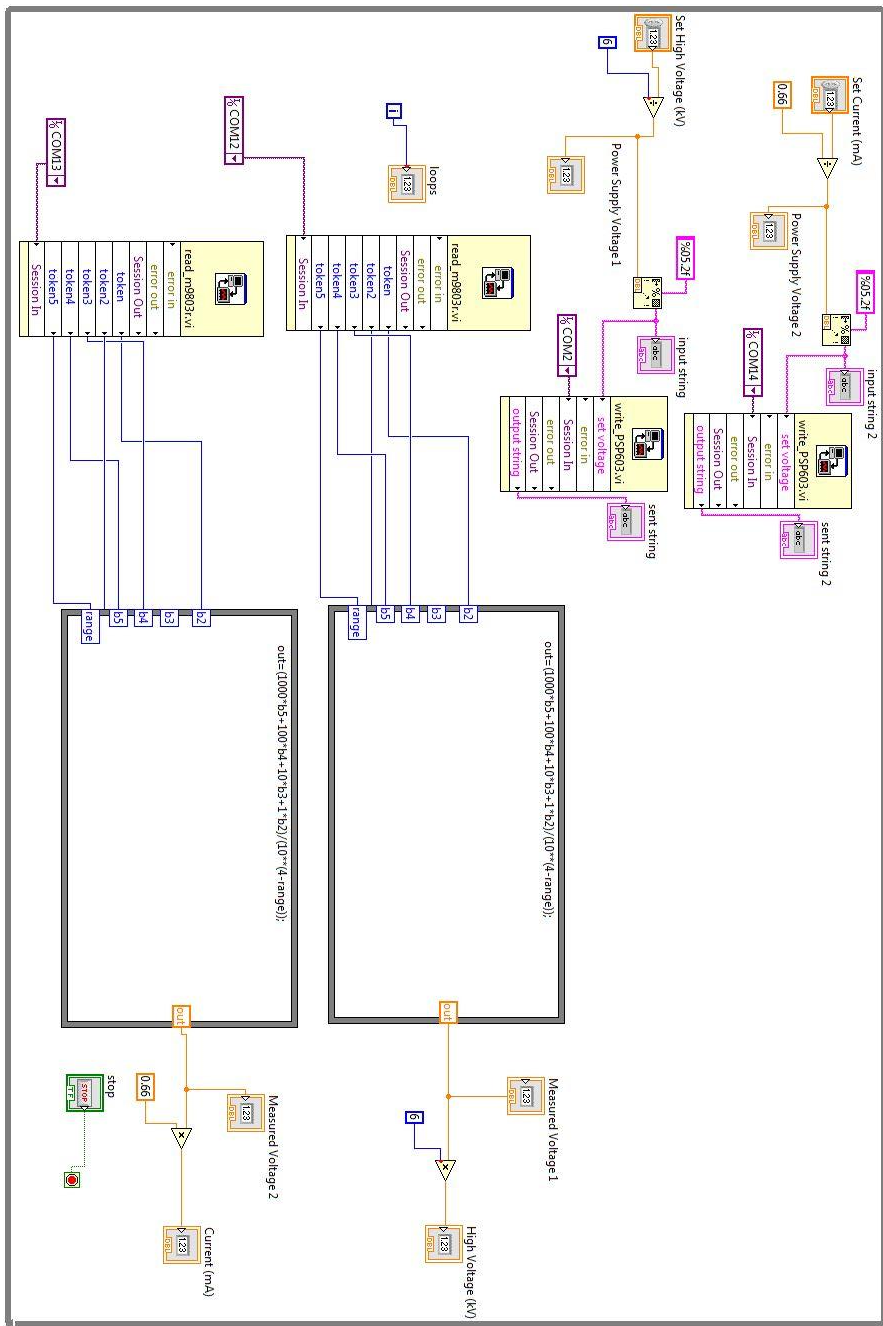


Figure 17. A LabVIEW VI that reads two M9803R devices and writes to two PSP 603 devices using their respective subprograms. The bytes that were read from the M9803R devices are assembled together and output to the screen.

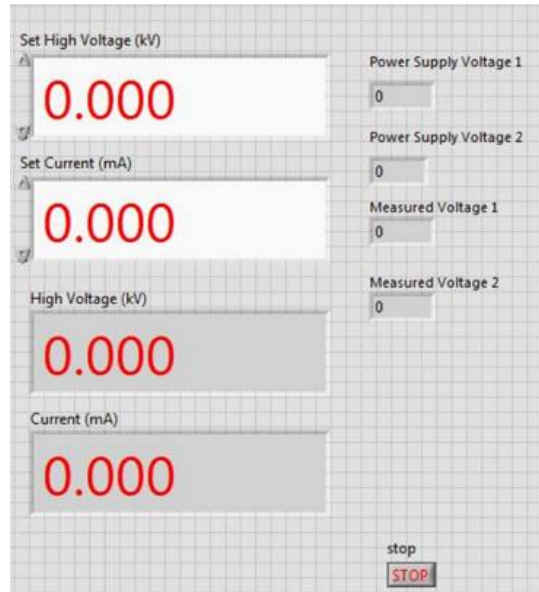


Figure 18. Front panel for the combined LabVIEW VI. The voltage and current limit can be set using the two upper left numeric controls while the two lower left numeric indicators display the output voltage and current. The numeric indicators on the right side show the voltages currently on the LCD screens of the PSP 603 and M9803R devices.

### 3.3 Controlling and Monitoring Chamber Pressure

The pressure inside of the fusor chamber is controlled and monitored using an Apex AX-MC-50SCCM-D mass flow controller and an InstruTech CCM501 cold-cathode ion gauge, respectively. Both of these devices are operated remotely in a similar fashion to the PSP 603 and M9803R discussed above. The details of the operation of both of these devices are discussed below.

#### 3.3.1 Remote Operation of Mass Flow Controller

The Apex AX-MC-50SCCM-D mass flow controller can be controlled remotely on a network using RS-232 from a Portserver TS 4 MEI. The mass flow controller connects to the Portserver TS 4 MEI through

a MiniDIN-DB9 cable connected to a DB9-RJ45 cable which is connected to the Portserver. The three wires in the cable are attached to the connectors according to Table 3.

Table 3. The required pin configuration for the RS-232 cable connecting the Apex AX-MC-50SCCM-D mass flow controller to the Portserver.

MiniDIN Pin	DB-9 Pin	RJ-45 Pin	Function
3	3	4	RS-232 Input (TxD)
5	2	5	RS-232 Output (RxD)
8	5	6	Ground

The mass flow controller is operated remotely using the LabVIEW program shown in Figure 19. The mass flow controller has a maximum flow rate of 50 SCCM, or 50 standard cubic centimeters per minute. To adjust the set-point of the mass flow controller, a number between 0 and 65535 is written to it, where 64000 represents the full-scale flow range. To determine the value for a given flow-rate, the following formula is used

$$Value = \frac{Set\ Point \times 64000}{50} \quad (3.1)$$

where 50 is the full-scale flow rate (in units of SCCM) for this particular mass flow controller.

The mass flow controller has two modes of operation, streaming and polling. In streaming mode, data is continuously output to the computer screen, and if a program like Hyperterminal is used, to the screen. In polling mode, data is only output when requested. To communicate with the mass flow controller, polling mode was used since LabVIEW is being used for data collection. In LabVIEW, data is not typically read from a device continuously, so the ability to read one line at a time is desirable. In order to set the mass flow controller in polling mode, its address "A" is concatenated to the beginning of the value for the set-point. This whole string is written to the mass flow controller using a LabVIEW Instrument Assistant to change the set-point and set the mass flow controller in polling mode.

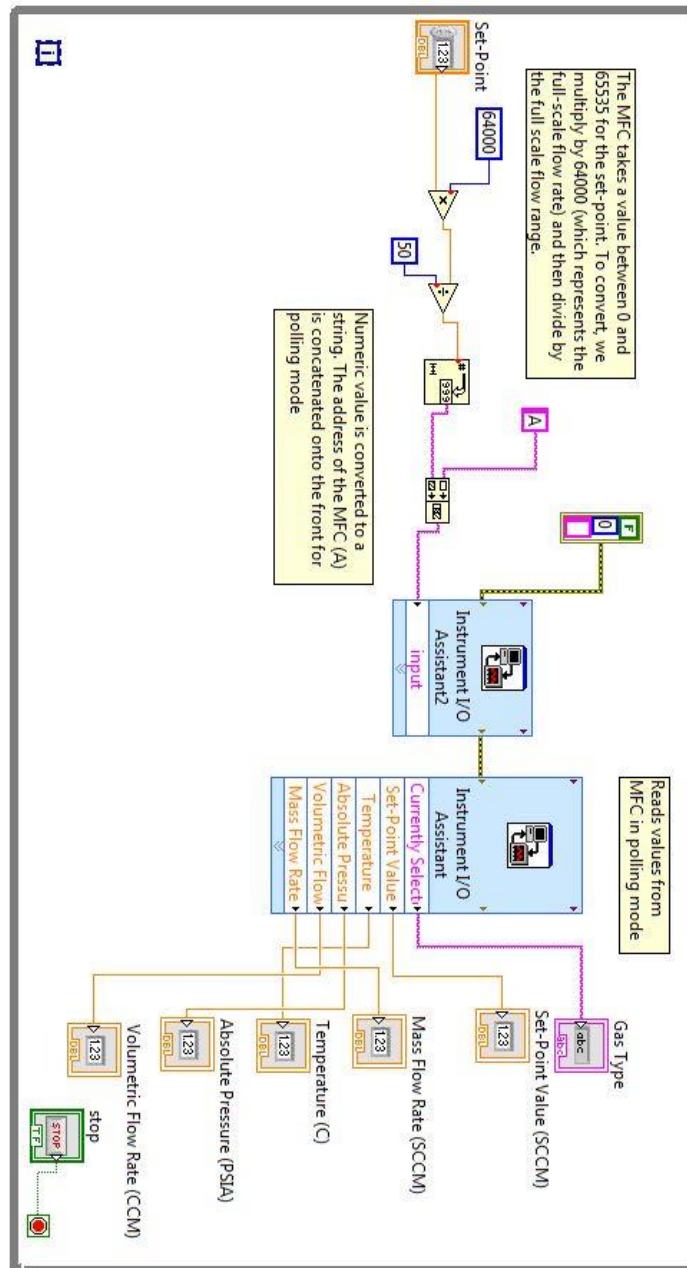


Figure 19. A LabVIEW program that adjusts the set-point of the Apex AX-MC-50SCCM-D mass flow controller by sending a string with a desired value along with the letter A to indicate polling mode. Data are then read from the device by parsing the received string based on whitespace. Finally, the parsed tokens are displayed to the screen.

Data are then read from mass flow controller using a LabVIEW Instrument Assistant, which when specified with the correct settings such as baud rate, parity, etc., will facilitate writing to and reading from any device. The mass flow controller returns a string with a format “+014.70 +025.00 +02.004 +02.004 2.004 Air”. The first entry is the absolute pressure in PSIA, the second is the temperature in °C, the third is the volumetric flow rate, the fourth is the mass flow rate, the fifth is the current set-point, and the sixth is the currently selected gas. The Instrument Assistant parses this string into tokens using the whitespace as the separator. The passed tokens are then output to the screen separately. This whole process is inside a while loop to continuously update and read measurements from the mass flow controller.

### 3.3.2 *Calibration of the Mass Flow Controller*

The pressure inside of the fusor chamber is adjusted by changing the set-point of the mass flow controller. The set point is in units of SCCM, or standard cubic centimeters per second, which represents a flow rate. The correlation between the flow rate and the pressure inside of the chamber was not known since this depends on factors such as the size of the chamber, the gas being used, leaks and the outgas rate for the chamber, and the pump speed of both the forepump and diffusion pump. Therefore, it was measured in order to calibrate the operating pressure range of the fusor, with the results shown in Figure 20. The results are then used when manually changing the set-point to give some indication of the approximate pressure after the set-point is changed so that the pressure is not increased or decreased too rapidly.

### 3.3.3 *Remote Operation of the Cold-Cathode Ion Gauge*

Most of the devices used with the fusor can be operated remotely using the RS-232 interface. However, the InstruTech CCM501 cold-cathode ion gauge communicates using the RS-485 interface, which uses two lines to write and two to read rather than one line for each as well as using different voltages. The Digi Portserver TS 4 MEI also supports this mode of communication. The required pin configuration

needed to communicate with the CCM501 is listed in Table 4. Additionally, the pin settings for the Portserver's EIA485 (Half) Duplex mode is listed in Table 4.

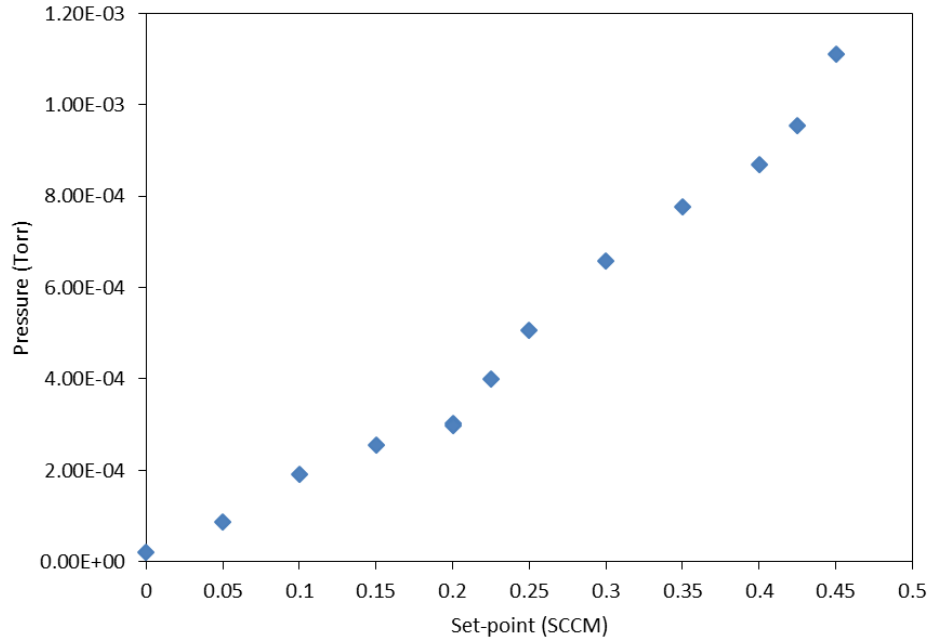


Figure 20. Pressure in the chamber as a function of the set-point of the mass flow controller for a chamber filled with air. From set-points of 0-0.425 SCCM, the pressure ranged from  $2.00 \times 10^{-5}$  Torr to  $9.55 \times 10^{-4}$  Torr.

Table 4. The pin configuration needed to connect the InstruTech CCM501 cold-cathode ion gauge to the Digi Portserver TS 4 MEI using a DB15-RJ50 cable.

CCM501 Pin	Function	Portserver Pin	Function
1	RS-485 DATA B(+) Input/Output	1	TxD-
		2	RxD-
2	Ground	4	Ground
3	RS-485 DATA A(-) Input/Output	5	TxD+
		6	RxD+

The program to operate the CMM501 is shown in Figure 21, while the front panel is shown in Figure 22. The first if statement checks to see if the high voltage is turned on or off. Depending on the state of the switch, a different string is sent to the CCM501, indicating for it to turn on or off. The status of the CCM501 is then checked to see if it is on or off. If on, the pressure is read. If an error is received, the program keeps trying to read until a valid string is read, or until 30 attempts at which the program is stopped. If the pressure gauge is off, then the pressure is not read and just set to 0 as a default value.

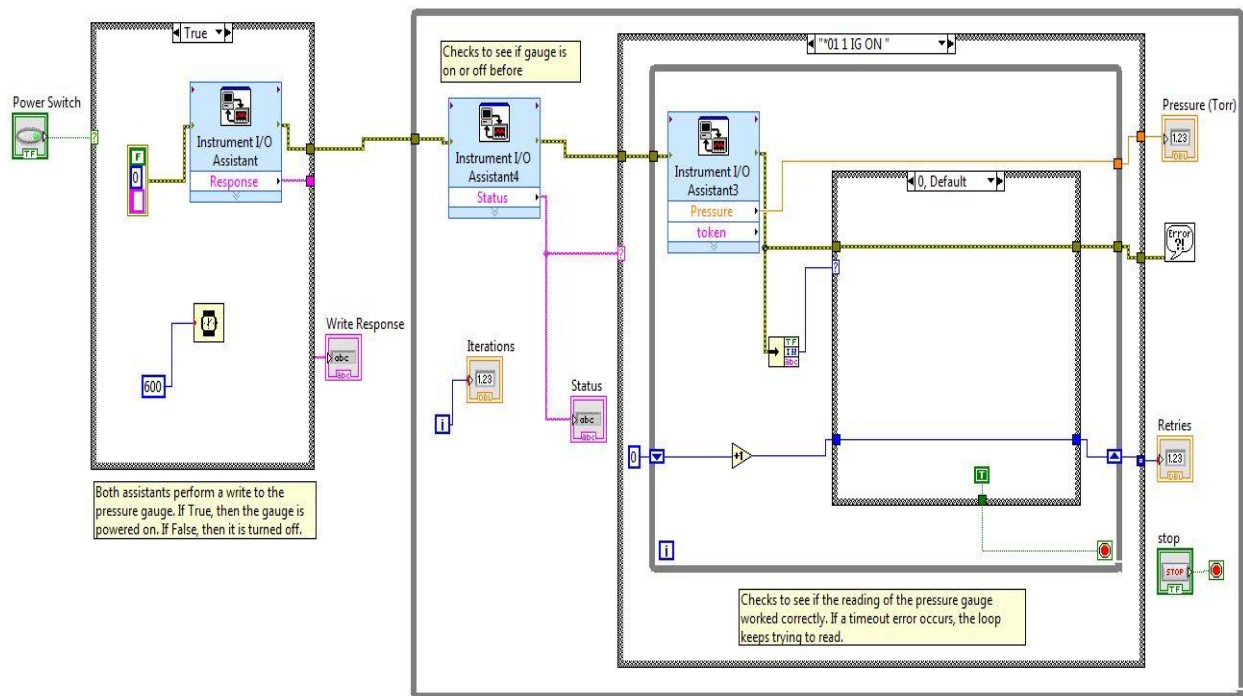


Figure 21. LabVIEW VI that both turns the high voltage for the InstruTech CCM501 pressure gauge and reads the pressure from the gauge. The pressure gauge is first turned on or off before entering a while loop for continuous reading of the pressure. Before reading, the status of the device is checked to prevent trying to read a pressure while off.

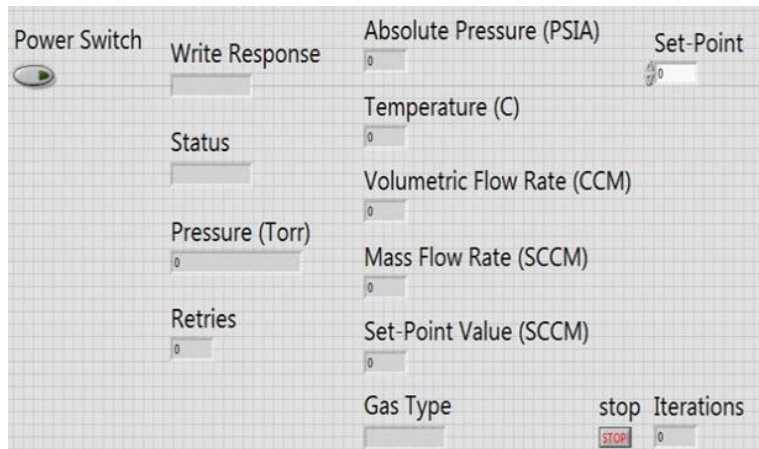


Figure 22. Front panel for operating the both the Apex AX-MC-50SCCM-D mass flow controller and InstruTech CCM501. The CCM501 can be turned on or off using the power switch, while the pressure and status is displayed in the numeric indicators on the left side. The set-point of the mass flow controller can be changed using the numeric control, while all of the important measurements are read and displayed in the numeric indicators on the right side.

## Chapter 4

### RESULTS AND CONCLUSIONS

#### 4.1 Results from Low-Pressure Air

The remote operation of the fusor was tested using low-pressure air as the gas inside of the chamber. Although all the parts had been previously tested individually, this test was to see how everything worked together. Furthermore, the test was also to see if changes could be made quickly enough to control the experiment due to the latency in writing to and reading all of the sensors. The pressure and voltage needed to be quickly changed in order to maintain a plasma as the high voltage is raised. Typical results are displayed in Figures 23, 24, 25. At low initial voltages, there was negligible current, indicating that there was no plasma. Once a plasma was formed, the current increased roughly linearly with voltage as shown in Figure 23, eventually plateauing at around 1.01 mA even though the maximum output current for the Bertan is 3.3 mA.

After the current plateaued, the output voltage still increased with the set voltage. However, after increasing the set voltage to a certain value, the actual voltage output started to deviate from the desired output voltage. This indicated that the voltage was limited by something, most likely the current limit of the power supply. This process is shown in Figure 24. Notice that when the set voltage reached around 7 kV, the output voltage did not increase any further. In order to increase the output voltage, the pressure was lowered in order to lower the current in the plasma. The pressure in the chamber was lowered slowly until the output voltage once again equaled the set voltage as shown in Figure 25. If the pressure was lowered too much, the plasma was lost due to there not being enough ions in the chamber. Once the set voltage was attained, then the voltage was further increased until the output voltage again started to be limited. In order to reach the maximum voltage of the Bertan, this process was repeated, slowly increasing the voltage. At high voltages, the current still remained at 1.01 mA and x-rays were produced,

which were detected using a Geiger counter near the port with the hot-cathode ion gauge, which has thin glass allowing x-rays to penetrate out into the air

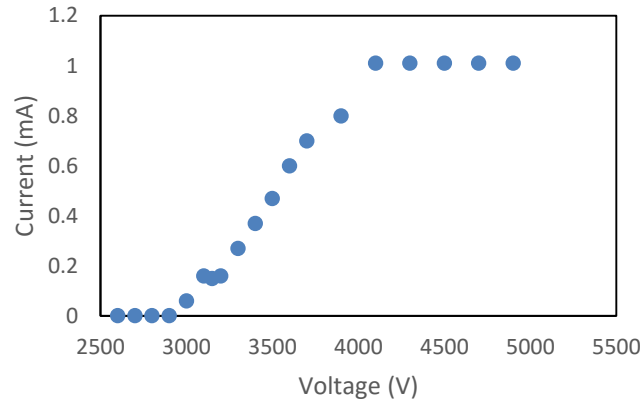


Figure 23. The current versus voltage for an air-filled chamber at a pressure of 4.8 mTorr. Once a plasma was formed (indicated by a non-zero current) the current increased approximately linearly with the voltage until around 4000 V.

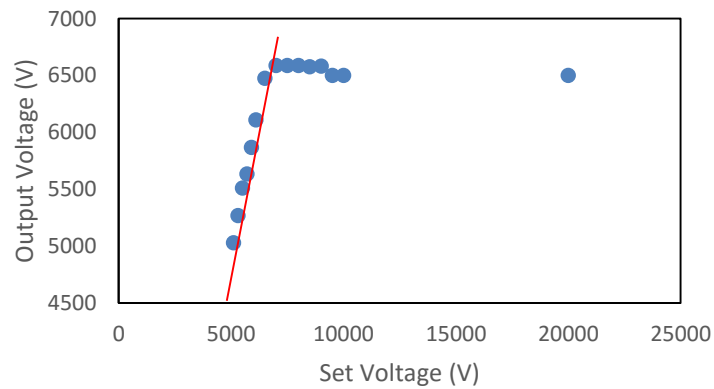


Figure 24. The output voltage versus set voltage for an air-filled chamber at 4.8 mTorr. After the current reached its maximum at 1.01 mA, the actual voltage output started to deviate from the set voltage. The red line represents the linear relationship  $y = x$ .

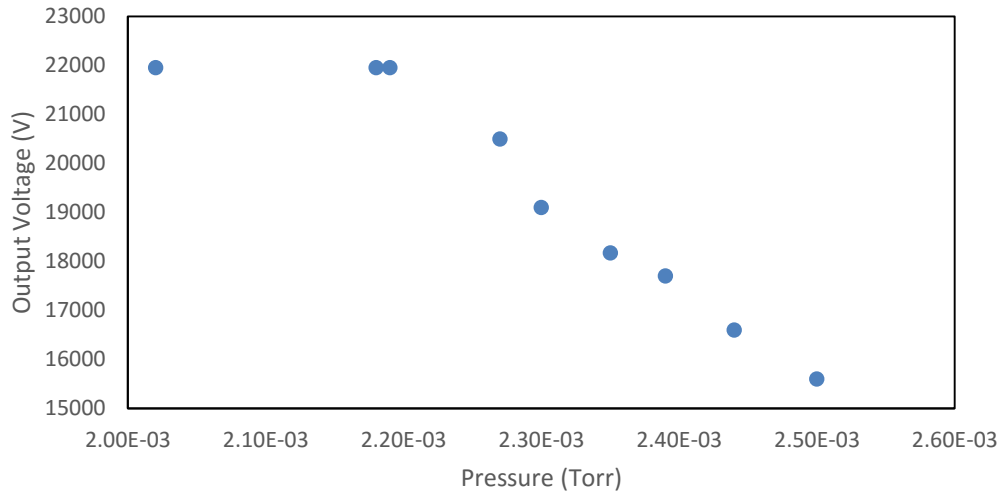


Figure 25. The output voltage versus the pressure for an air-filled chamber at a set voltage of 22 kV. In order to get the output voltage to equal the set voltage, the pressure was slowly lowered.

After successful operation of the fusor with low-pressure air, the fusor was filled with hydrogen and another test was performed. Although the test with air was successful, the test with hydrogen was not. Plasma did not form in the chamber, but near the feedthrough where the high voltage line enters the chamber. Increasing the voltage further did not create ionization in the chamber, but only caused sparking in the feedthrough region. The electrical feedthrough was replaced with a Kurt J. Lesker EFT3013093 electrical power feedthrough, which has a conflat size of 2.75" and is rated up to 30,000 V. The distance from the high voltage line to the grounded chamber is larger due to this new feedthrough and the high voltage line is also surrounded by ceramic and is farther from the chamber walls. This will hopefully prevent ionization from occurring in the feedthrough although testing has not been done yet. If not, another potential fix is to include a filament inside of the chamber to produce electrons and aid in ionization.

## 4.2 Conclusions and Future Work

The implementation of remote operation for a Farnsworth-Hirsch fusor at Houghton College has been completed. The fusor is now operated using a Bertan Series 815 -30N high voltage power supply, that is able to be operated remotely through the use of external power supplies and multimeters, as well as an Instek CCM501 cold-cathode ion gauge and Apex AX-MC-50SCCM-D mass flow controller to monitor and control the pressure in the chamber, respectively. These devices are operated remotely through a combination of RS-232 and RS-485 serial interfaces over Ethernet and are controlled through LabVIEW VIs. The fusor was successfully operated remotely with low-pressure air in the chamber. Successful operation using low-pressure hydrogen has not been attained due to ionization occurring in the feedthrough rather than the chamber.

Future plans include fixing the chamber to achieve successful operation with hydrogen. Currently a new feedthrough has been attached but not tested. If the replacement feedthrough does not solve the problem, then a filament will be placed inside the chamber to produce electrons to ionize the gas. Once the fusor is tested with hydrogen, the next course of action is operation of the fusor using deuterium gas in order to study D-D reactions including looking at the energy produced as well as the cross-section of the D-D plasma. Neutrons, although few should be produced by this reaction as indicated by Figure 26. These neutrons will be measured with a bonner sphere to indicate whether or not fusion is occurring. The measurement of the neutrons will also be used to decide the safety of the device and of the people operating it.

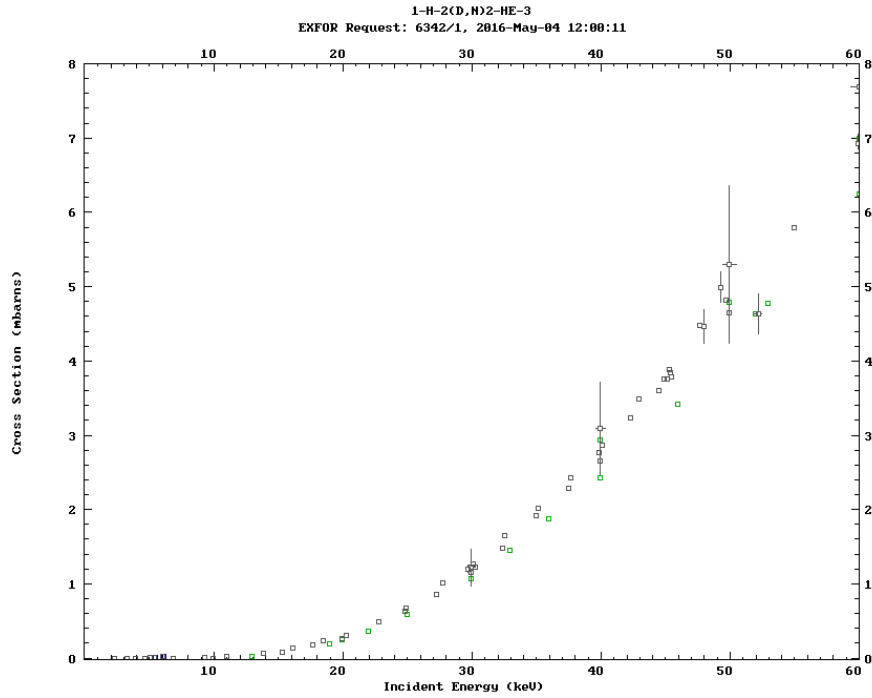


Figure 26. The cross section for  ${}^2\text{H}(\text{d},\text{n}){}^3\text{He}$  as a function of incident energy. In the Farnsworth-Hirsch fusor, the incident energy will be less than 30 keV, but will be enough for the  ${}^2\text{H}(\text{d},\text{n}){}^3\text{He}$  reaction to occur since the cross-section for 20-30 keV of incident energy is between approximately 0.4 and 1.2 mbarns. Since the  ${}^2\text{H}(\text{d},\text{n}){}^3\text{He}$  reaction releases neutrons, the Farnsworth-Hirsch fusor is capable of producing neutrons. Figure retrieved from EXFOR using data from [17][18][19][20][21][22][23][24].

## References

- [1] S. Pfalzner, *An Introduction to Inertial Confinement Fusion* (Taylor and Francis, New York, 2006), p. 1-17.
- [2] J.D. Lawson, Proc. Phys. Soc. B. **70** (1957).
- [3] S. Earnshaw, Trans. Camb. Phil. Soc. **7**, 97 (1842).
- [4] G.H. Miley and S.K. Murali, *Inertial Electrostatic Confinement Fusion: Fundamentals and Applications* (Springer, New York, 2014), p.31-37.
- [5] P.T. Farnsworth, U.S. Patent No. 3,258,402 (28 June 1966).
- [6] P.T. Farnsworth, U.S. Patent No. 3,386,883 (4 June 1968).
- [7] R.L. Hirsch and G.A. Meeks, U.S. Patent No. 3,530,497 (22 September 1970).
- [8] R.W. Bussard, Fusion Science and Technology **19**, 273-293 (1991).
- [9] J.F. Santarius, G.L. Kulcinski, R.P. Ashley, et al., Fusion Science and Technology **47**, 1238-1244 (2005).
- [10] Y. Takeyama, R. Thomas, G. H. Miley, presented at Trends in Fusion Research, Washington, D.C., 2005 (unpublished).
- [11] J. Sved, presented at International Topical Meeting on Nuclear Research Applications and Utilization of Accelerators, Vienna, 2009 (unpublished).
- [12] P. Schatzkin, Fusor.net, 2016.
- [13] T.H. Rider, Physics of Plasmas. **2**, 1853-1872 (1995).
- [14] D.R. Nicholson, *Introduction to Plasma Theory* (John Wiley & Sons, New York, 1983), p.37-43.
- [15] E. Sonnendrucker, "Numerical Methods for the Vlasov Equation", Lecture Notes, Technical University of Munich, 2013 (unpublished).
- [16] I. Love, Undergraduate Thesis, Houghton College, 2014.
- [17] V.A. Davidenko, A.M. Kucher, I.S. Pogrebov, et al., Atomnaya Energiya **1957**, 7 (1957) (EXFOR 1168.002).
- [18] V.M. Bystritsky, V.V. Gerasimov, A.R. Krylov, et al., Bull.Russian Academy of Sciences **74**, 531 (2010) (EXFOR 1083.003).
- [19] M.A. Hofstee, A.K. Pallone, F.E. Cecil, et al., Nuclear Physics A **688**, 527 (2001) (EXFOR 1511.002).
- [20] U. Greife, F. Gorris, M. Junker, et al., Zeitschrift fuer Physik A **351**, 107 (1995) (EXFOR 1171.002).

- [21] A.S. Belov, V.E. Kusik, Yu.V. Ryabov, *Nuovo Cimento A* **103**, 1647 (1990) (EXFOR 1299.002).
- [22] R.E. Brown, N. Jarmie, *Phys. Rev. C* **41**, 1391 (1990) (EXFOR 0109.005).
- [23] The First Research Group, *High Energy Physics and Nucl. Physics* **9**, 723 (1985) (EXFOR 0025.002).
- [24] D.L. Booth, G. Preston, P.F.D. Shaw, *Proc. Physical Society A* **69**, 265 (1956) (EXFOR 0033.004).